

THE MASS-LOSS RETURN FROM EVOLVED STARS TO THE LARGE MAGELLANIC CLOUD. II. DUST PROPERTIES FOR OXYGEN-RICH ASYMPTOTIC GIANT BRANCH STARS

BENJAMIN A. SARGENT¹, S. SRINIVASAN², M. MEIXNER¹, F. KEMPER³, A. G. G. M. TIELENS⁴, A. K. SPECK⁵, M. MATSUURA^{6,7}, J.-PH. BERNARD⁸, S. HONY⁹, KARL D. GORDON¹, R. INDEBETOUW^{10,11}, M. MARENGO¹², G. C. SLOAN¹³, AND PAUL M. WOODS³

¹ Space Telescope Science Institute, 3700 San Martin Drive, Baltimore, MD 21218, USA; sargent@stsci.edu

² Institut d'Astrophysique de Paris, 98 bis, Boulevard Arago, Paris 75014, France

³ Jodrell Bank Centre for Astrophysics, Alan Turing Building, School of Physics and Astronomy, The University of Manchester, Oxford Road, Manchester, M13 9PL, UK

⁴ Leiden Observatory, P.O. Box 9513, NL-2300 RA Leiden, The Netherlands

⁵ Physics & Astronomy Department, University of Missouri, Columbia, MO 65211, USA

⁶ Institute of Origins, Department of Physics and Astronomy, University College London, Gower Street, London WC1E 6BT, UK

⁷ Institute of Origins, Mullard Space Science Laboratory, University College London, Holmbury St. Mary, Dorking, Surrey RH5 6NT, UK

⁸ Centre d'Étude Spatiale des Rayonnements, 9 Av. du Colonel Roche, BP 44346, 31028 Toulouse Cedex 4, France

⁹ Laboratoire AIM, CEA/DSM-CNRS-Université Paris Diderot DAPNIA/Service d'Astrophysique Bât. 709, CEA-Saclay F-91191 Gif-sur-Yvette Cédex, France

¹⁰ Department of Astronomy, University of Virginia, P.O. Box 400325, Charlottesville, VA 22904, USA

¹¹ National Radio Astronomy Observatory, 520 Edgemont Road, Charlottesville, VA 22903, USA

¹² Department of Physics and Astronomy, Iowa State University, Ames, IA 50011, USA

¹³ Department of Astronomy, Cornell University, Ithaca, NY 14853, USA

Received 2009 August 20; accepted 2010 April 26; published 2010 May 21

ABSTRACT

We model multi-wavelength broadband *UBVIJHK_s* and *Spitzer* IRAC and MIPS photometry and Infrared Spectrograph spectra from the SAGE and SAGE-Spectroscopy observing programs of two oxygen-rich asymptotic giant branch (O-rich AGB) stars in the Large Magellanic Cloud (LMC) using radiative transfer (RT) models of dust shells around stars. We chose a star from each of the bright and faint O-rich AGB populations found by earlier studies of the SAGE sample in order to derive a baseline set of dust properties to be used in the construction of an extensive grid of RT models of the O-rich AGB stars found in the SAGE surveys. From the bright O-rich AGB population, we chose HV 5715, and from the faint O-rich AGB population we chose SSTSAGE1C J052206.92–715017.6 (SSTSAGE052206). We found the complex indices of refraction of oxygen-deficient silicates from Ossenkopf et al. and a power law with exponential decay grain size distribution like what Kim et al. used but with γ of -3.5 , a_{\min} of $0.01 \mu\text{m}$, and a_0 of $0.1 \mu\text{m}$ to be reasonable dust properties for these models. There is a slight indication that the dust around the faint O-rich AGB may be more silica-rich than that around the bright O-rich AGB. Simple models of gas emission suggest a relatively extended gas envelope for the faint O-rich AGB star modeled, consistent with the relatively large dust shell inner radius for the same model. Our models of the data require the luminosity of SSTSAGE052206 and HV 5715 to be $\sim 5100 L_{\odot}$ and $\sim 36,000 L_{\odot}$, respectively. This, combined with the stellar effective temperatures of 3700 K and 3500 K, respectively, that we find best fit the optical and near-infrared data, suggests stellar masses of $\sim 3 M_{\odot}$ and $\sim 7 M_{\odot}$. This, in turn, suggests that HV 5715 is undergoing hot-bottom burning and that SSTSAGE052206 is not. Our models of SSTSAGE052206 and HV 5715 require dust shells of inner radius ~ 17 and ~ 52 times the stellar radius, respectively, with dust temperatures there of 900 K and 430 K, respectively, and with optical depths at $10 \mu\text{m}$ through the shells of 0.095 and 0.012, respectively. The models compute the dust mass-loss rates for the two stars to be $2.0 \times 10^{-9} M_{\odot} \text{yr}^{-1}$ and $2.3 \times 10^{-9} M_{\odot} \text{yr}^{-1}$, respectively. When a dust-to-gas mass ratio of 0.002 is assumed for SSTSAGE052206 and HV 5715, the dust mass-loss rates imply total mass-loss rates of $1.0 \times 10^{-6} M_{\odot} \text{yr}^{-1}$ and $1.2 \times 10^{-6} M_{\odot} \text{yr}^{-1}$, respectively. These properties of the dust shells and stars, as inferred from our models of the two stars, are found to be consistent with properties observed or assumed by detailed studies of other O-rich AGB stars in the LMC and elsewhere.

Key words: circumstellar matter – infrared: stars – stars: AGB and post-AGB

Online-only material: color figures

1. INTRODUCTION

Asymptotic giant branch (AGB) stars are low- to intermediate-mass ($\lesssim 8 M_{\odot}$) stars that have reached the last stages of their lives as stars. In this phase of an AGB star's life, the star expels its own circumstellar material, forming dust grains as the material moves away from the star, dragging the gas with it through momentum coupling. The photospheric abundance of carbon relative to oxygen determines whether the ejected dust will be of oxygen-rich (O-rich) or carbon-rich (C-rich) composition (Höfner 2009). This ejected dust is

subsequently added to the interstellar medium (ISM) surrounding the star. At least some dust grains from AGB stars in our Galaxy survive their residence in the ISM and are incorporated into planet-forming disks around young stars, as must have happened for our solar system (Gail et al. 2009; Nittler 2009).

It is desirable to determine the relative contributions to the mass budget from different sources of dust in a galaxy. Studies of dusty stars in our own Galaxy are difficult, as shorter-wavelength observations, necessary to constrain emission from the star and hot dust, are hampered by the high extinction along lines of sight through the disk of the Milky Way (e.g., see Schultheis

et al. 2003). Further, the often unknown extent of extinction by intervening dust hampers precise distance determinations, which, in turn, affects determining AGB star luminosities. Blommaert et al. (2006) studied the mass loss of AGB stars in the Galactic Bulge; however, their surveys did not include lines of sight through the Galactic midplane, which can have very high extinction. The Surveying the Agents of a Galaxy’s Evolution (SAGE) *Spitzer Space Telescope* (Werner et al. 2004) Legacy project was designed to study the life cycle of baryonic matter in the Large Magellanic Cloud (LMC; Meixner et al. 2006). Among other advantages of surveying the LMC include a low average reddening of $E(B - V) \sim 0.075$ (Schlegel et al. 1998). Also, because of the inclination angle of the LMC, all stars in the LMC are at roughly the same distance from us (see discussion by Meixner et al. 2006), which eases determination of their luminosities.

Infrared Array Camera (IRAC; Fazio et al. 2004) SAGE observations found millions of stars in the LMC surveys. Of the $\sim 32,000$ of these millions that were classified as evolved stars brighter than the tip of the red giant branch (RGB) in the LMC by Blum et al. (2006), over half ($\sim 17,500$) of them were found to be O-rich AGB stars. Another ~ 7000 were found to be C-rich AGB stars, and ~ 1200 were found to be “extreme” AGBs of undetermined chemistry. C-rich and extreme AGB stars amongst the SAGE sample will be explored in detail elsewhere (see Srinivasan 2009); here, we focus instead on O-rich AGB stars. The O-rich AGB stars were found to divide into two populations (Blum et al. 2006), a bright one and a faint one (see also Srinivasan et al. 2009, hereafter Paper I).

To determine the relative contribution to the mass budget of the LMC from O-rich AGB stars, we desire to construct detailed radiative transfer (RT) models of each of these stars found in the SAGE survey. However, these models require adequate dust optical properties in order to compute reliable dust mass-loss rates to be used in obtaining total mass-loss rates. Numerous detailed RT studies have been conducted on O-rich AGB stars with an eye toward determining the optical properties of the silicate dust produced by such stars. Volk & Kwok (1988) used the RT code DUSTCD (Leung 1975, 1976a, 1976b; Spagna & Leung 1983) to model AGB stars, constructing their own dust opacity function in the process, for which they found the more massive AGB stars typically had $10 \mu\text{m}$ silicate features in absorption. Schutte & Tielens (1989) also used code by Leung (1975, 1976a, 1976b) to model AGB stars, noting the classical problem of requiring more near-infrared wavelength ($1 < \lambda/\mu\text{m} < 8$) continuum absorption than observed in typical terrestrial silicates to model the AGB stars successfully and proposing “color centers” in astronomical silicates as a possible solution (among others). Simpson (1991) constructed RT shell models to try to determine the dust emissivities for different groups of stars observed by the low-resolution spectrometer on *IRAS* to have silicate emission. Suh (1999) used CSDUST3 (Egan et al. 1988) in modeling O-rich AGBs to construct optical constants sets for two different silicates—warm and cool, which were later used by Suh (2004) to model the mass loss of pulsating AGB stars with low and high mass-loss rates. Kemper et al. (2002) revisited the problem of the lack of near-infrared continuum opacity in AGB stars by modeling the OH/IR star OH 127.8+0.0 using the RT code MODUST (Bouwman et al. 2000; Kemper et al. 2001; Bouwman 2001), concluding the near-infrared continuum arises from metallic iron. Recently, Heras & Hony (2005) have used the one-dimensional RT code DUSTY (Ivezic et al. 1999) to model O-rich AGB stars with optically

thin dust envelopes, finding evidence for various oxides and silicates.

IRAC and Multiband Imaging Photometer for *Spitzer* (MIPS; Rieke et al. 2004) SAGE observations of some of the brightest sources were followed up with *Spitzer* Infrared Spectrograph (IRS; Houck et al. 2004) spectra as part of the SAGE-Spectroscopy (SAGE-Spec; PI: F. Kemper) *Spitzer* Legacy program (Kemper et al. 2010). These spectra, along with IRAC and MIPS photometry, plus shorter-wavelength visible and near-infrared photometry obtained from other sources, allow detailed spectral energy distributions (SEDs) to be constructed for a small number of stars.

Here, we determine dust grain properties that will allow reasonable RT model fits to the observed SEDs and spectra of O-rich AGB populations (Blum et al. 2006). This search for typical dust properties is preparation for future work to determine the mass-loss contribution of O-rich AGB stars in the LMC to its total mass budget. Ultimately, we wish to obtain the mass-loss rate for each of thousands of O-rich AGB stars in the LMC (found in the SAGE surveys) by RT modeling of its SED, which includes dust emission beyond $3.6 \mu\text{m}$ wavelength. This paper focuses on the RT modeling of a representative star from each of the bright and faint O-rich AGB populations, in order to find reasonable dust grain properties to use for more extensive later modeling of O-rich AGB stars. A similar study has been undertaken for a C-rich AGB star (Srinivasan et al. 2010, hereafter Paper III).

2. OBSERVATIONS

As discussed above, Blum et al. (2006) noted the presence of two distinct populations of O-rich AGB stars in the SAGE sample of the LMC, a faint population and a bright population. Allowing for differences in the dust properties between the populations, we chose a representative star from each population. For the best constraints on the dust emissivity at mid-infrared wavelengths, we chose to model from each of the bright and faint populations a star with redder [8.0]–[24] colors than over half of its respective population, as redder colors suggest more prominent dust feature emission. However, we did not want the [8.0]–[24] color to be too red, in order to avoid modeling an anomalous source. Also, we wanted to model stars with SAGE-Spec IRS spectra, to provide tight constraints on the silicate emission features of our representative stars. From the bright O-rich AGB star population, we chose HV 5715 (SAGE-Spec ID 82). From the faint O-rich AGB star population, identified by an “F” in the [24], [8.0]–[24] color–magnitude diagram (CMD) of Blum et al. (2006), we chose SSTISAGE1C J052206.92–715017.6 (hereafter, SSTSAGE052206; SAGE-Spec ID 96). The K_s magnitudes for HV 5715 and SSTSAGE052206 are 9.064 and 11.203, both well above the tip of the RGB of $K_s = 11.98$ (Cioni et al. 2000), confirming the status of these stars as AGBs. These two stars have amongst the highest signal-to-noise ratio (S/N) in the 10 and $20 \mu\text{m}$ silicate emission features of the O-rich AGB stars observed in the SAGE-Spec program (Paul M. Woods et al. 2010, in preparation).

Each of the two O-rich AGB stars we chose to model had $<10\%$ agreement between the fluxes at 5.8, 8.0, and $24 \mu\text{m}$ synthesized from its 5–37 μm *Spitzer*-IRS spectrum and the corresponding observed IRAC or MIPS *Spitzer* photometry. The IRS spectra of these two stars show clear silicate emission, testifying to their O-rich nature. In the Two Micron All Sky Survey (2MASS) K_s , J – K_s CMD of Nikolaev & Weinberg (2000),

SSTSAGE052206 occupies region F, identified by Nikolaev & Weinberg (2000) as O-rich AGB stars of intermediate age. The other star, HV 5715, was located in region G of the 2MASS CMD plotted by Nikolaev & Weinberg (2000), corresponding to young AGB stars that have such a high mass that hot-bottom burning (HBB; Boothroyd & Sackmann 1992) prevents them from becoming or staying C-rich.

2.1. Photometry and Variability

Using MACHO data, Wood et al. (1999) found five sequences when plotting luminosity index versus $\log(P)$, where P is the period. They identify sequence “C” with Miras and show the variability of the stars in this sequence to be consistent with pulsation in the fundamental mode. With a larger data set, Fraser et al. (2005) resolved the sequence Wood et al. (1999) identified as “B” into two sequences, which they name sequences 2 and 3. Both Fraser et al. (2005) and Fraser et al. (2008) show sequences 1 (sequence C of Wood et al. 1999), 2, and 3 to have lightly populated, nearly vertical extensions at the bright ends of the sequences (the lowest K_s magnitudes).

MACHO data (Fraser et al. 2008) for HV 5715¹⁴ indicate multi-periodic variability, with primary and secondary periods of 415.97 and 211.06 days, respectively, with corresponding peak-to-peak MACHO blue-band amplitudes of 0.8 and 0.66, respectively. On plots of K_s versus $\log(\text{primary period})$ by Fraser et al. (2008), the point corresponding to the primary period of HV 5715 falls within the edge of the nearly vertical extension to sequence 1. The point corresponding to the secondary period of HV 5715 lies on the side of sequence 2 closest to sequence 3. The plots of peak-to-peak amplitude versus $\log(\text{period})$ and primary-to-secondary period ratio versus $\log(\text{primary period})$ shown by Fraser et al. (2008) are also consistent with the primary period of HV 5715 belonging to sequence 1.

SSTSAGE052206 matches the coordinates and average V and I magnitudes for OGLE-LMC-LPV-46603, identified as an “OGLE Small Amplitude Red Giant” (OSARG) in the long period variable (LPV) list of the OGLE-III Catalog of Variable Stars¹⁵ (Soszyński et al. 2009). The catalog entry for OGLE-LMC-LPV-46603 gives primary, secondary, and tertiary periods of 81.24, 399.8, and 69.08 days, respectively, and their corresponding amplitudes (half of the peak-to-peak amplitude) for the light curve at I band are 0.061, 0.047, and 0.038 mag, respectively. According to Figure 2 of Fraser et al. (2008), its primary period and its K_s magnitude place it in between sequences 3 and 2, slightly closer to 3 than to 2, while its secondary period places it between sequences 1 and D. Both Figures 8 and 9 of Fraser et al. (2008) show SSTSAGE052206 to be very close to the “one-year artifact,” which perhaps suggests some caution in the secondary period they find for this star of 399.8 days. Fraser et al. (2008) note that OSARGs are closely related to RGB and E-AGB stars. SSTSAGE052206 is only somewhat brighter than the tip of the RGB (see our earlier discussion), which suggests it to be in the earlier stages of its AGB star phase.

2MASS (Skrutskie et al. 2006) JHK_s and *Spitzer* IRAC 3.6, 4.5, 5.8, and 8.0 μm data for HV 5715 and SSTSAGE052206 come from the SAGE Winter 2008 IRAC Catalog, and *Spitzer* MIPS 24 μm data come from the SAGE Winter 2008 MIPS

24 μm Catalog. Both catalogs are available on the NASA/IPAC Infrared Science Archive web site.¹⁶ See Meixner et al. (2006) and Blum et al. (2006) for more details on the SAGE epoch-1 point-source catalog, from which we obtain the data for HV 5715 and SSTSAGE052206. We applied the zero-point offsets recommended by Cohen et al. (2003) to the 2MASS data. At shorter wavelengths, we use *UBVI* data from the Magellanic Clouds Photometric Survey (Zaritsky et al. 1997) for these two objects. We correct the *UBVIJHK_s* photometry for foreground extinction (for more details, see Cioni et al. 2006). The IRAC and MIPS photometry is not corrected for extinction, as the correction is negligible at those wavelengths.

To this photometry, for HV 5715 we add from Glass (1979) B , V , R_{ck} , and I_{ck} (the last two being in the Cape Kron system; see Cousins 1976), and two epochs of J , H , K , and L photometry. In addition, we add *BVR* photometry from Rebeiro et al. (1983) and J and H photometry from IRSF (Kato et al. 2007). To SSTSAGE052206, we add IRSF photometry at J , H , and K_s bands. We correct this additional photometry (except for the L -band flux) for extinction by linear interpolation in $\log(A_\lambda)$ versus $\log(\lambda)$ space, where A_λ is the extinction at wavelength λ , of the extinction law used by Cioni et al. (2006). Due to the multi-periodic nature of HV 5715 and both the multi-periodic nature and weak variability of SSTSAGE052206, we do not attempt to construct a single-phase SED for either star from multi-epoch photometry. Instead, for each star we plot the photometry from all epochs on the same SED.

2.2. Spectroscopy

Data from the S15.3 and S17.2 pipelines for the Short-Low (SL) and Long-Low (LL) modules, respectively, were obtained from the SSC for SSTSAGE052206 (AOR no. 22422528) and HV 5715 (AOR no. 22419456). After reducing the spectra using techniques described by Kemper et al. (2010), SL spectra were scaled up to match LL spectra in flux near 14.3 μm .

3. MODELS

3.1. 2Dust Radiative Transfer Models

There are many RT codes from which to choose. Many of the RT codes mentioned in the introduction assume spherical symmetry. This is not as much a concern for very optically thin dust shells. Every grain in such shells receives starlight with almost no extinction, and the radiation it scatters or emits thermally toward the observer likely experiences even less extinction due to the typically decreasing extinction efficiency of carbonaceous and O-rich dust toward longer wavelengths. However, our interests include very dusty AGB stars, for which cases the geometry of the circumstellar dust does play a strong role in the heating and emergent SEDs of the stars. In anticipation of our future modeling of very dusty AGB stars that may have nonspherical dust shell geometries, we use the RT code 2Dust (Ueta & Meixner 2003), which allows nonspherical axisymmetric circumstellar dust shell geometries.

3.1.1. Dust Shell Geometry

For the current study, we simply assume spherical symmetry of the dust around the star, noting both the weakness of the mid-infrared flux relative to the flux at 1 μm and the lack of silicate absorption features in the IRS spectra for both stars (see

¹⁴ See the MACHO light curves for MACHO id 49.6132.10 at the coordinates of HV 5715 of right ascension 79:54623, declination -67:4467 available under “Lightcurve Search” at <http://www.macho.anu.edu.au/Data/MachoData.html>

¹⁵ See <http://ogledb.astrouw.edu.pl/~ogle/CVS/>

¹⁶ <http://irsa.ipac.caltech.edu/data/SPITZER/SAGE/>

Figures 1 and 2) suggest optically thin dust shells. We assume a $1/r^2$ density fall for the dust in the shell, which is expected for constant mass-loss rate. The inner radius (R_{\min}) and outer radius (R_{\max}) are parameters that define the size of the shell. R_{\min} is varied for a best fit. Heras & Hony (2005) found the outer radius of the dust shell, R_{\max} , in their AGB models to be not easily constrained, and suggested a lower limit for their sample of 100 times the inner radius of the dust shell. We set the outer radius of the dust shell for both models at a thousand times the inner shell radius (Volk & Kwok 1988), which is important for catching all the contributions from the dust shell to the $24\ \mu\text{m}$ MIPS flux.

3.1.2. Stellar Temperature

To represent the stellar photosphere emission, we use PHOENIX models (Allard et al. 2000) for stars of one solar mass and subsolar metallicity ($\log(Z/Z_{\text{Sun}}) = -0.5$) to match determinations of the metallicity of the LMC ($Z/Z_{\text{Sun}} \sim 0.3\text{--}0.5$; see Westerlund 1997). We favor PHOENIX models, as they include millions of lines from water vapor and other molecules critical for modeling cool, late-type stars as we do here with AGB stars. To give the best fit to the visible and near-infrared photometry, we use photosphere models corresponding to stellar effective temperatures, T_{eff} , of $3500\ \text{K} \pm 100\ \text{K}$ and $3700\ \text{K} \pm 100\ \text{K}$ for HV 5715 and SSTSAGE052206, respectively. The uncertainty in the effective temperature was estimated to be about 100 K for both stars, as PHOENIX models are given in 100 K increments, and the photosphere models with the next highest and lowest effective temperatures gave marginally acceptable fits to the optical and near-infrared photometry. Those stellar photosphere models with effective temperatures 200 K greater or lesser than the ones we used provided noticeably worse fits to the optical and near-infrared photometry. We note here that selection of the best stellar photosphere model will be much more difficult when constructing RT models of highly optically thick dust shells for later model grids (B. Sargent et al. 2010, in preparation) than for the two stars modeled here, as the optical and near-infrared colors will be affected by the optically thick dust shells.

3.1.3. Stellar Luminosity

PHOENIX models were only available for stars of one solar mass, but (as we discuss in Section 4.5) our stars are more massive. We therefore chose to use for modeling each of our two stars the one solar mass PHOENIX model with the nearest value of $\log(g)$ to what we estimate for the star. To determine the correct value of $\log(g)$ to use for each star, where g is the gravitational acceleration at the star's surface in CGS units, we obtained a first guess for stellar radius and mass by assuming the star's mass is one solar mass. We then adjusted the assumed stellar radius to a value that resulted in a good fit of the photometry from U - through K_s -band wavelengths. From the luminosity of the resultant stellar photosphere and T_{eff} , we placed our two stars on isochrones and determined stellar masses of ~ 7 and $\sim 3\ M_{\odot}$ for HV 5715 and SSTSAGE052206, respectively (see discussion in Section 4.5). With stellar mass and our first guess at stellar radius, we determined values of $\log(g)$ for HV 5715 and SSTSAGE052206 of -0.15 and $+0.43$, respectively, so we used the PHOENIX models with $\log(g)$ values logarithmically nearest these values: 0.0 and $+0.5$, respectively.

To fit the observed photometry, we scale the fluxes of the $T_{\text{eff}} = 3500\ \text{K}$, $\log(g) = 0.0$ PHOENIX model for HV 5715

by 9.74, and we scale the fluxes of the $T_{\text{eff}} = 3700\ \text{K}$, $\log(g) = 0.5$ PHOENIX model for SSTSAGE052206 by 3.48. The luminosities of the resultant photospheres we use in our modeling are $\sim 36,000\ L_{\odot} \pm 4000\ L_{\odot}$ and $\sim 5100\ L_{\odot} \pm 500\ L_{\odot}$ for HV 5715 and SSTSAGE052206, respectively. We estimate the relative uncertainties on the luminosity for each of HV 5715 and SSTSAGE052206 to be about 10%. Should the fluxes for either star be scaled by more than 10% from their current values, the fits to the overall SEDs and spectra would grow noticeably worse. To obtain the stellar radii, this means scaling the radii of the unscaled PHOENIX models for HV 5715 and SSTSAGE052206 by $\sqrt{9.74}$ and $\sqrt{3.48}$, respectively. Since $L = \sigma T^4 4\pi R^2$, the 10% relative uncertainties on the luminosities imply $\sim 5\%$ uncertainties on the stellar radii, assuming we have the correct stellar effective temperatures. Supporting the assumption of our assumed subsolar metallicity is the fact that the only plot in Figure 1 of Marigo et al. (2008) for which both HV 5715 and SSTSAGE052206 would have effective temperatures and luminosities corresponding to O-rich AGB stars is the plot corresponding to $Z = 0.008$. This is about 0.42 times solar, consistent with Westerlund (1997). Here, we note that if we scaled the stellar photosphere model for HV 5715 to fit the lowest fluxes in each band for which there is photometry from multiple epochs, we would obtain a luminosity of $\sim 31,000\ L_{\odot}$, about 15% lower than the value we use (which instead fits the highest fluxes in the bands that have multi-epoch photometry). The stars are assumed to be 50 kpc away (Feast 1999).

3.1.4. Expansion Velocity (v_{exp})

The dust is assumed to be moving away from the star for each model at a terminal velocity of $10\ \text{km s}^{-1}$ (see Wood et al. 1992; Marshall et al. 2004). When we changed this parameter, it had no visible effect upon the SED, so we cannot constrain this parameter from our data. The dust mass-loss rate is affected by this parameter, as it is linearly proportional to the expansion velocity by design of the **2Dust** code. For HV 5715, the expansion velocity of $10\ \text{km s}^{-1}$ we adopted is consistent with Figure 4 of Marigo et al. (2008), which plots expansion velocities for variable AGB stars versus their periods. There are few data points with primary periods as low as that of SSTSAGE052206 in Figure 4 of Marigo et al. (2008), but the three points with primary periods around or below 200 days have expansion velocities between ~ 9 and $\sim 17\ \text{km s}^{-1}$, which are consistent with the value of $10\ \text{km s}^{-1}$ we assume in our modeling. The Vassiliadis & Wood (1993) relation in that plot does not extend below primary periods of 200 days.

3.1.5. Dust Cross Sections and Sizes

The **2Dust** models were run in Harrington averaging (Harrington et al. 1988) mode, which means the dust cross sections used to represent the dust properties in RT were cross sections computed from weighted averages, with the weights being proportional to the grain surface area. We assumed isotropic scattering because we found it to give output SEDs almost indistinguishable from those computed assuming anisotropic scattering (using a modified Henyey–Greenstein phase function; see Cornette & Shanks 1992). Mie theory (Bohren & Huffman 1983) is used to compute the absorption and scattering cross sections and asymmetry factor, g , of the dust grains, assumed spherical in shape, around the AGB stars. However, real astrophysical dust grains are likely to be nonspherical (Bohren & Huffman 1983). The cross sections of spherical and nonspherical grains differ

Table 1
2Dust Model Parameters and Results

Parameter	HV 5715	SSTSAGE1C J052206.92 -715017.6
Star		
T_{eff} (K)	3500 ± 100	3700 ± 100
$\log(g)$	0.0	0.5
$\log(Z/Z_{\text{Sun}})^*$	-0.5	-0.5
$R_{\text{star}}(R_{\odot})$	520 ± 30	170 ± 10
$L_{\text{star}}(L_{\odot})$	$36\,000 \pm 4\,000$	$5\,100 \pm 500$
Dust grains		
ρ_{dust}^* (g cm^{-3})	3.3	3.3
γ^*	-3.5	-3.5
a_{min} (μm)	0.01 (0.0003, 0.08)	0.01 (0.0003, 0.09)
a_0 (μm)	0.1 (0.02, 0.3)	0.1 (0.02, 0.5)
Assumed values		
$R_{\text{max}}/R_{\text{min}}^*$	1000	1000
v_{exp}^* (km s^{-1})	10	10
Dust shell		
τ_{10}	0.012 (0.009, 0.015)	0.095 (0.07, 0.13)
$R_{\text{min}}(R_{\text{star}})$	52 (25, 93)	17 (9, 28)
$T_{d,\text{inner}}$ (K)	430 (310, 650)	900 (700, 1200)
\dot{M}_{dust} ($10^{-9} M_{\odot} \text{ yr}^{-1}$)	2.3 (1.1–4.1)	2.0 (1.1–3.1)
\dot{M}_{total} ($10^{-6} M_{\odot} \text{ yr}^{-1}$)	1.2 (0.2–6.5)	1.0 (0.2–5.2)

Notes. The photosphere model flux for HV 5715 was obtained by scaling the flux from the original photosphere model (which had $\log(g)$ of 0.0) by 9.74 and corresponding R_{star} by $\sqrt{9.74}$; for SSTSAGE052206, the original photosphere model (with $\log(g)$ of 0.5) flux was scaled by 3.48 and R_{star} by $\sqrt{3.48}$. A KMH grain size distribution $n(a) \propto a^{\gamma} e^{-a/a_0}$ (Kim et al. 1994) was used for both models. An asterisk (*) indicates a parameter was fixed, not determined from model fitting. Values in parentheses beside the best-fit values for τ_{10} , R_{min} , a_{min} , and a_0 are the allowable ranges of uncertainty of these parameters, as described in subsections of Section 3.1. Note also the gas-to-dust mass ratio assumed, 500, for computing the total mass-loss rate from the dust mass-loss rate is quite uncertain, as discussed in the text.

most in the resonances (features), as ensembles of nonspherical grains tend to give wider features, with the long-wavelength side of the features pushed to longer wavelengths (see Fabian et al. 2001; Min et al. 2005). This potential difference could cause a discrepancy between observed and modeled spectra. The dust grains were assumed to follow a Kim–Martin–Hendry (KMH)-like “power law with exponential decay (PED)” (Kim et al. 1994) grain size distribution, in which the number of grains of a given size is proportional to $a^{\gamma} e^{-a/a_0}$, where a is the grain radius, a_0 sets the exponential decrease in number of grains to large sizes, and a_{min} is the minimum grain size. When a is much smaller than a_0 , the grain size distribution acts approximately as a^{γ} , so γ is fixed at -3.5 (after Mathis et al. 1977), and a_{min} and a_0 were allowed to be free parameters. We found $a_{\text{min}} = 0.01 \mu\text{m}$ and $a_0 = 0.1 \mu\text{m}$ to provide good fits of models to observed data.

3.1.6. Fitting Procedure

To obtain the best-fit model for each of our two stars, we generally began by determining stellar properties (stellar effective temperature and luminosity) first, dust shell properties next, and dust grain properties last. All other properties were fixed, as described previously in the text. Sometimes we had to iterate and loop through stellar, dust shell, and dust grain properties again. After computing hundreds of models through such iteration, we found an acceptable combination of stellar,

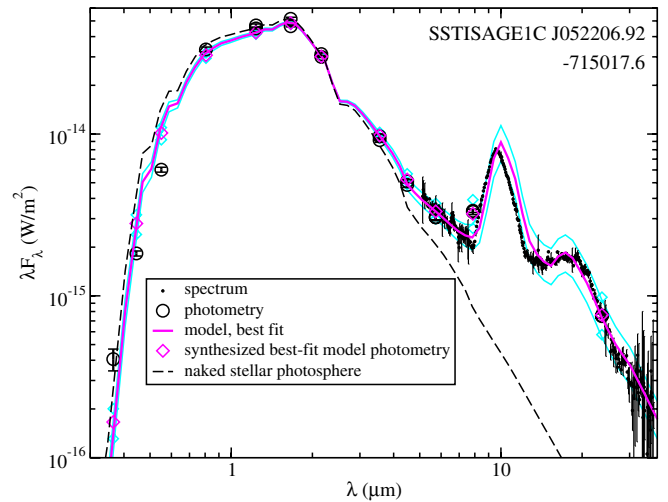


Figure 1. 2Dust model fit to the SED of SSTSAGE052206. The small black dots with vertical lines through them are the IRS spectrum data points with error bars, the large open circles with error bars are the observed photometry (see Section 2.1 for sources of photometry), the model fit is the magenta thick solid line, the large open magenta diamonds are the photometry synthesized from the model, and the black dashed line is the naked stellar photosphere model. Components in cyan are the model and synthetic photometry for models with optical depth at $10 \mu\text{m}$, τ_{10} , at the extremes of its allowable range. The lower cyan curve and set of points corresponds to $\tau_{10} = 0.07$, and the upper cyan curve and set of points corresponds to $\tau_{10} = 0.125$. This demonstrates how the uncertainty for τ_{10} was determined.

(A color version of this figure is available in the online journal.)

dust shell, and dust grain properties for both SSTSAGE052206 and HV 5715.

We would begin by selecting an unscaled PHOENIX stellar photosphere model of effective temperature and $\log(g)$ value that would give fluxes as close as possible to those of our stars. We then scaled the photosphere models in flux up to match the SED fluxes, changing to using a PHOENIX model of differing $\log(g)$ value as needed (described previously). Then, the dust shell optical depth at $10 \mu\text{m}$ (τ_{10}), was increased to the approximate level to match the flux in the 10 and $20 \mu\text{m}$ features. Later, the dust shell inner radius (R_{min}) was varied to obtain both the correct relative fluxes in the 10 and $20 \mu\text{m}$ features and the correct slope of the underlying near- and mid-infrared continuum ($\lambda < 8 \mu\text{m}$ and $13 \mu\text{m} < \lambda < 15 \mu\text{m}$). Lastly, a_{min} and a_0 were varied to try to improve the fit. The fits were judged successful when the 10 and $20 \mu\text{m}$ peak fluxes were matched, the near- and mid-infrared continuum in the model was as close as possible to that in the data, and the broadband fluxes at optical and near-infrared wavelengths were matched as closely as possible. The details of the model properties are given in Table 1. Figures 1 and 2, respectively, show the observed data and best-fit models for SSTSAGE052206 and HV 5715.

We note here that the IRS spectrum of HV 5715 may be well fitted by our model over its entire wavelength range (5–38 μm) only if we fit just the maximum flux of each band for which there is photometry from multiple epochs. This suggests that the IRS spectrum for HV 5715 was obtained near its maximum in phase. As this object has multiple periods and, as a result, has quite a complex light curve (see Section 2.1), we do not attempt to correct either the IRS spectrum or any photometry for phase. We note the spread in fluxes seems to be small for the IRAC bands, grows slightly larger for I , J , H , and K bands, and grows larger still for the V and B bands. We further note that Vjih et al. (2009), in their study

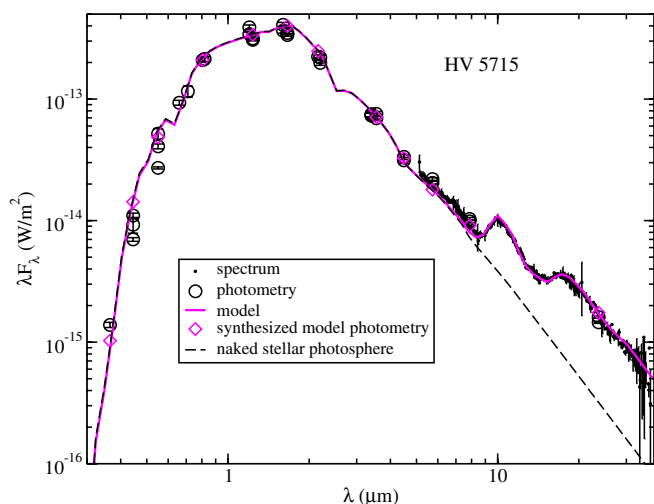


Figure 2. 2Dust model fit to the SED of HV 5715. Same meaning of symbols as for Figure 1, without the cyan curves and points.

(A color version of this figure is available in the online journal.)

of variability at mid-infrared wavelengths, list neither HV 5715 nor SSTSAGE052206 as variable, consistent with their infrared variability being relatively small. This increased amplitude in variability with shorter wavelengths may be intrinsic to the source. As Reid & Goldston (2002) summarize, Celis (1978), building on earlier studies (e.g., Pettit & Nicholson 1933; Smak 1964), noted the increasing amplitude in variability of Mira pulsating variables to shorter wavelengths. However, based on the low number of measurements we have in each of the concerned bands, we draw no further conclusions regarding the wavelength dependence of the variability of our stars. The single observed *U*-band flux we do have for HV 5715 (and SSTSAGE052206, for that matter) is higher than the flux synthesized from our model. The reason for these *U*-band discrepancies is unknown, but it does support fitting only the maximum fluxes in the other bands of HV 5715, as fitting the median or mean of those bands would decrease the model flux at *U* even further below the observed flux than it already is. The variability of SSTSAGE052206 is much smaller, so its model agrees quite well with both its photometry from all epochs and its IRS spectrum.

The dust shell inner radius (R_{\min}) and especially the dust shell optical depth at $10\ \mu\text{m}$ (τ_{10}) have the greatest effects on the fluxes and colors of the output SEDs. The grain size parameters, a_{\min} and a_0 , were of great interest, as we seek acceptable grain properties through modeling of HV 5715 and SSTSAGE052206 to use in extensive RT modeling of O-rich evolved stars in the SAGE sample in the future. All four parameters— R_{\min} , τ_{10} , a_{\min} , and a_0 —were left free, to be determined by our RT modeling. To gauge the range, a parameter could vary and the overall fit of model to data remain acceptable, the fluxes longward in wavelength of $3\ \mu\text{m}$ were allowed to deviate by one to three times the uncertainties, as estimated by eye, while keeping all other parameters at their best-fit value (Table 1). Figure 1 demonstrates this estimation of uncertainty by eye for the τ_{10} parameter for SSTSAGE052206, giving as cyan curves the models obtained with τ_{10} set to the extremes of its allowable range (see values in parentheses in Table 1 beside the best-fit value for this parameter). The uncertainties on the other free parameters for SSTSAGE052206 and all four free parameters for HV 5715 were determined in the same way.

We list in Table 1 the uncertainties in R_{\min} , τ_{10} , a , and a_0 determined by eye in parentheses beside their best-fit values. We save more exact determinations of uncertainties of model parameters and a detailed investigation of degeneracy of pairs of free model parameters for our future study of the entire model grid. For now, we suggest the reader see Speck et al. (2009) for a further discussion on RT modeling parameter degeneracy and sensitivity to certain parameters.

3.1.7. Dust Grain Composition

Models using many different sets of refractory indices were constructed, but few were found to provide an overall good fit to the SED. Models using refractory indices of amorphous silicates made from the “sol-gel” method (Jäger et al. 2003) were computed, but these silicates were found to achieve insufficient temperatures to match the infrared fluxes in the SEDs. This was also true of the refractory indices of amorphous pyroxene of “cosmic” composition (Jäger et al. 1994) and of the amorphous pyroxenes of Dorschner et al. (1995) for stoichiometries with $\text{Fe}/(\text{Mg}+\text{Fe})$ values less than ~ 0.5 . For the refractory indices for amorphous pyroxenes from Dorschner et al. (1995) with $\text{Fe}/(\text{Mg}+\text{Fe})$ values of 0.5 and 0.6, the dust temperatures were more reasonable and the model spectra more closely matched the observed spectra longward in wavelength of $8\ \mu\text{m}$, but the near-infrared continuum of the model shortward of $8\ \mu\text{m}$ was very much below the observed continuum at those wavelengths in the observed data (both IRAC photometry and IRS spectrum) for both HV 5715 and SSTSAGE052206. Also, the $20\ \mu\text{m}$ feature was too strong. Both sets of amorphous olivine refractory indices from Dorschner et al. (1995) gave reasonable grain temperatures and reasonable fits to the IRS spectra longward of $8\ \mu\text{m}$ and provided closer matches to the observed near-infrared continuum. However, the extinction at *I* and *J* bands was too large for the model of SSTSAGE052206, and the $20\ \mu\text{m}$ features were still too strong compared to the IRS spectra. The refractory indices of Suh (1999) for “warm” and “cool” silicates and those of Ossenkopf et al. (1992) for O-rich silicates were found to give moderately acceptable fits to the shapes of the 10 and $20\ \mu\text{m}$ emission features in the IRS spectra, but the peak-to-continuum ratio for the $20\ \mu\text{m}$ features in the models was too large, compared to the IRS spectra.

We found the refractory indices of oxygen-deficient silicates by Ossenkopf et al. (1992) to give the best fits of models to data, giving a physically reasonable dust shell geometry when fitting the models to the SEDs and giving the best overall fits to the 10 and $20\ \mu\text{m}$ features and to the near-infrared continuum in the spectra. In order to use these constants, we had to add wavelength coverage, as the shortest wavelength of the oxygen-deficient silicate refractory indices of Ossenkopf et al. (1992) was $0.4\ \mu\text{m}$. To these Ossenkopf et al. (1992) refractory indices, we added indices between 0.2 and $0.4\ \mu\text{m}$ determined by interpolating between the n and k values for Ossenkopf et al. (1992) at $0.4\ \mu\text{m}$ and the n and k values for the “astronomical silicate” of Draine & Lee (1984) at $0.1718\ \mu\text{m}$. Increased average grain size would flatten the $10\ \mu\text{m}$ feature and make it wider, pushing its long-wavelength side to longer wavelengths (see Min et al. 2005), which is needed neither for HV 5715 nor (especially) for SSTSAGE052206. In addition, the fits would not be improved by incorporating real nonspherical astrophysical grains because an ensemble of nonspherical grains will push the long-wavelength sides of the features to longer wavelengths (Min et al. 2005), which is not needed. Overall, the fits to the 10 and $20\ \mu\text{m}$ features for HV 5715 and SSTSAGE052206 are not

perfect, but we are not aiming to fit the detailed shapes of the dust emission features in the spectra. We also note our best fits are likely not unique; however, our goal here is to find good dust grain properties to use in RT modeling of O-rich AGB stars, with reasonable assumptions for the stellar properties and other dust shell properties. Instead, we aim to obtain good overall fits to the SEDs and save determination of details like grain shape distribution for future studies.

3.1.8. Synthetic Photometry

In order to compare our models, which have high wavelength resolution, to broadband photometry, we synthesized broadband fluxes, which we include in Figures 1 and 2 as diamonds, from our models. We describe here how we synthesized photometry for the bands for which photometry was readily available in the SAGE catalogs; for the additional photometry we plot for HV 5715, we did not synthesize photometry from our model to compare. For each of the bands of the *UBVI* photometry, we obtained the quantum-efficiency (QE) based response function by multiplying the QE of the Direct CCD Camera¹⁷ by the transmission function of the band.¹⁸ The band fluxes for the *UBVI* bands were then obtained by computing the isophotal flux (see Equation (5) of Tokunaga & Vacca 2005). For each of the 2MASS *JHK_s* bands, photon-counting relative spectral response (RSR) functions were obtained¹⁹ and used to compute isophotal fluxes (see discussion in Appendix E.4 of Bessell et al. 1998, regarding QE-based versus photon-counting response functions and computing band fluxes). For the IRAC and MIPS photometry points, the fluxes were obtained using the IDL routine *spitzer_synthphot*.²⁰

3.2. SSTSAGE052206 Gas Model

A small feature appears in the spectrum of SSTSAGE052206 at 6.6 μm . A simple isothermal slab model of water vapor emission with a temperature of 1000 K, column density of 10^{18} cm^{-2} , and microturbulent velocity of 3 km s^{-1} (Table 2), using a line list from Partridge & Schwenke (1997) convolved to $R \sim 90$ was obtained using a model from the *spectrafactory* web site²¹ (see discussion by Cami et al. 2010). We note the 6.6 μm feature is present for water vapor of temperatures greater than 500 K in these models, so the 1000 K temperature is not well constrained. The assumed emitting surface was a circle whose emitting area is $2200 R_{\odot}$ in radius ($\sim 13 R_{\text{star}}$). This is only $\sim 4 \text{ AU}$ inward of the inner radius of the dust shell for this star (Table 1), and it supports the large dust shell inner radius we find from modeling the dust emission.

A carbon dioxide emission model was similarly constructed to fit the emission feature at 14.9 μm . In studies of Galactic

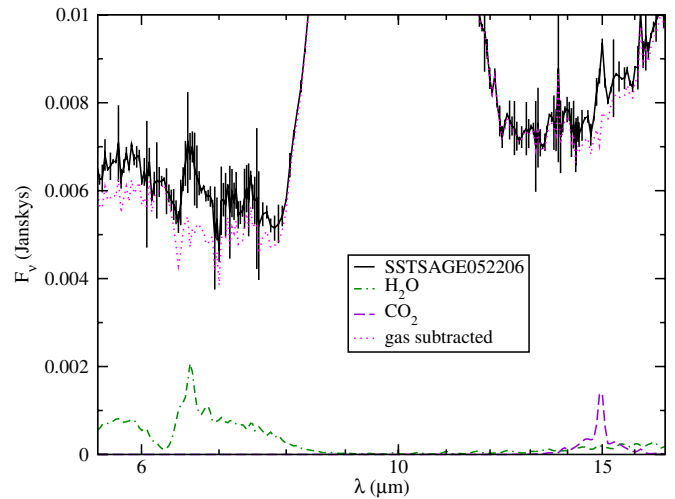


Figure 3. Spectrum of SSTSAGE052206 is compared to models of CO_2 and H_2O gas emission. The H_2O model is the green dot-dash-dash line, the CO_2 model is the purple dashed line, the IRS spectrum of SSTSAGE052206 is the solid black line with error bars, and SSTSAGE052206 spectrum minus both gas models is the dotted magenta line with no error bars.

(A color version of this figure is available in the online journal.)

O-rich AGBs, it was suggested by Justtanont et al. (1998) that stars with enhanced mass-loss rates would show little in the way of CO_2 emission. Sloan et al. (2003) showed that CO_2 emission strength in O-rich AGB stars was correlated with the strength of the 13 μm dust feature, which was found to be stronger in semi-regular variable stars than Miras. There is no 13 μm dust feature in SSTSAGE052206, and there are none of the other CO_2 lines either, suggesting weak CO_2 emission in SSTSAGE052206 more like that of a Galactic Mira star. We obtained a model spectrum from the *spectrafactory* web site to construct an isothermal slab model for 10^{17} cm^{-2} of CO_2 at 500 K (Table 2) convolved to the same spectral resolution as the water vapor spectrum, using a line list from Rothman et al. (2005). The emission was assumed to come from a circular area of radius $6000 R_{\odot}$ ($\sim 35 R_{\text{star}}$). This is qualitatively consistent with the picture presented by Cami (2002) that the CO_2 feature originates further from the star than the H_2O feature. H_2O and CO_2 features were also seen in the O-rich Mira star R Cas by Markwick & Millar (2000), who find their results consistent with a model that includes a pulsation shock.

Being variable and near the maximum in its light curve may explain the CO_2 and H_2O features in the spectrum of SSTSAGE052206 being in emission. At maximum, the greater luminosity of the star may heat up the circumstellar gas further away from the star. This would result in emission from gas in front of a negligible background surpassing absorption by the parts of the same gas cloud (at the same temperature) that happen to lie in the line of sight between star and observer, resulting in net emission features from the gas (for more, see Cami 2002). Indeed, the H_2O line-forming region is larger at maximum phase (Matsuura et al. 2002). H_2O emission from the extended atmosphere and circumstellar gas fill the H_2O absorption from the photosphere. However, because the photospheric H_2O has a higher excitation temperature than the H_2O in the outer atmosphere or circumstellar shell, and because photospheric absorption is so strong, H_2O emission from the outer shells is insufficient to fill the photospheric absorption completely (Tsuji et al. 1997). Indeed, the 6 μm H_2O band is usually observed in absorption (Tsuji 2001).

¹⁷ Available at

<http://www.lco.cl/lco/telescopes-information/irenee-du-pont/instruments/specs/du-pont-telescope-direct-ccd-camera-ccd>. This was extrapolated to 0.3 μm . Also, the QE was assumed to linearly drop to zero from its value at 0.84 μm wavelength, the last wavelength provided on the QE graph, to 1.13 μm , the wavelength corresponding to a photon energy of 1.1 eV, which is the energy of the band gap of silicon.

¹⁸ The transmission functions of the *B* and *V* bands were obtained from <http://www.lco.cl/lco/telescopes-information/irenee-du-pont/instruments/website/direct-ccd-manuals/direct-ccd-manuals/3x3-filters-for-ccd-imaging> using the Harris *B* and Harris *V* filter profiles, which are LC-3013 and LC-3009, respectively. The filter transmission profiles for *U* and *I* bands were obtained from I. Thompson (2009, private communication).

¹⁹ http://www.ipac.caltech.edu/2mass/releases/allsky/doc/sec6_4a.html

²⁰ For software and instructions, see

<http://ssc.spitzer.caltech.edu/dataanalysis/tools/cookbook/10/>

²¹ <http://www.spectrafactory.net>

Table 2
SSTSAGE052206 Gas Model Parameters

Parameter	H ₂ O	CO ₂
T_{gas} (K)	1000	500
N_{gas} (cm ⁻²)	10 ¹⁸	10 ¹⁷
v_{turb} (km s ⁻¹)	3	3
$R_{\text{slab}}(R_{\text{star}})$	13	35

Notes. T_{gas} is the temperature of the isothermal gas slab, N_{gas} is the gas column density into the slab, v_{turb} is the microturbulent velocity of the gas, and R_{slab} is the radius (expressed in stellar radii; for the stellar radii, see Table 1) of the emitting area, assumed circular, of the slab. The gas models are convolved to a spectral resolution of 90.

Cami (2002) did show that when the 14.9 μm CO₂ feature was in emission, other gas molecules' features would also tend to be more in emission, hypothesizing more extended gas envelopes in these cases. Perhaps SSTSAGE052206 has a very extended envelope, resulting in the water vapor features being in emission.

As can be seen from the gas emission models in Figure 3, only water vapor contributes with any significance to the near-infrared continuum. Even so, it contributes at less than the 10% level, so the dust emission is responsible for most of the continuum emission in excess of that from the stellar photosphere shortward of 8 μm . To lower the near-infrared continuum to account for this minute water vapor emission shortward of 8 μm would require either slightly increasing R_{min} or slightly decreasing any of τ_{10} , a_{min} , or a_0 . The contribution to continuum emission from CO₂ is negligible, so it is of no concern regarding better fitting the near-infrared continuum.

4. DISCUSSION

4.1. Dust Composition

Figures 1 and 2 show that the models for both SSTSAGE052206 and HV 5715 provide overall acceptable fits to the observed spectra and SEDs. The peak fluxes of the 10 and 20 μm features are fairly well matched. This is important, according to Justtanont et al. (2005), for deriving the mass-loss rate. We also note the oxygen-deficient silicates by Ossenkopf et al. (1992) we used were designed to have similar optical properties to “astronomical silicates” empirically constructed to fit previous observations of AGBs and other astrophysical sources. The problem of needing sufficient near-infrared ($\lambda < 8 \mu\text{m}$) continuum opacity has been identified for other O-rich AGB stars, such as OH 127.8+0.0 (Kemper et al. 2002), WX Psc (Decin et al. 2007), and HV 996 and IRAS 05558–7000 (van Loon et al. 1999). It is likely related to the problem of astronomical silicates needing to be “dirty” (absorptive) enough to heat sufficiently (Schutte & Tielens 1989), and has been solved elsewhere by increasing the imaginary part of the complex dielectric constant over near-infrared wavelengths to increase the continuum opacity in that range (e.g., Draine & Lee 1984). Since the Ossenkopf et al. (1992) silicates were based on previous empirically constructed “astronomical silicates,” the good fit of the underlying continuum shortward of 8 μm and between 13 and 15 μm is somewhat expected.

The 10 and 20 μm features in both model and data match very well in shape for HV 5715 and reasonably well for SSTSAGE052206. However, in detail the model and observed 10 and 20 μm features of SSTSAGE052206 disagree slightly. For SSTSAGE052206, the 10 μm feature in the model peaks a

few tenths of a micron longward in wavelength of the feature in the data, while the 20 μm feature in the model peaks a few tenths of a micron shortward in wavelength of the feature in the data. We have mentioned earlier the limitations of using Mie theory, which assumed spherical dust grains, and that real astronomical grains are likely not spherical (Bohren & Huffman 1983; Fabian et al. 2001; Min et al. 2005). However, the use of an ensemble of nonspherical shapes would tend to push both 10 and 20 μm features to longer wavelengths (e.g., see Fabian et al. 2001). This would improve the fit to the 20 μm feature of SSTSAGE052206, but it would worsen the fit to its 10 μm feature. Instead, we look to dust composition to explain these slight discrepancies in shape. Silicates with more silica-rich compositions, like pyroxenes, have 10 μm features centered at slightly shorter wavelengths than silica-poor silicates like olivines (Ossenkopf et al. 1992). More silica-rich compositions also tend to have 20 μm features shifted to longer wavelengths than silica-poor compositions (Dorschner et al. 1995; Jäger et al. 2003). This may suggest the silicates around SSTSAGE052206 may be slightly more silica-rich than those whose spectra were the basis of the “astronomical silicates” on which the Ossenkopf et al. (1992) silicates were based. By extension, this suggests the SSTSAGE052206 silicates are more silica-rich than the HV 5715 silicates. We note, though, that we are modeling only two sources. We will explore this issue further in future papers.

Subtracting the stellar photosphere used in our models from the observed spectrum, HV 5715 has a classification of SE6/SE7, while SSTSAGE052206 has a classification of SE8 in the classification system used by Sloan et al. (2003). Both stars have what Sloan et al. (2003) call classic silicate emission. More in-depth studies of the dust composition *via* the detailed spectral emission feature shapes await a future study. However, the dust properties used here provide overall satisfactory fits to the SEDs and spectra of SSTSAGE052206 and HV 5715 and represent a baseline for a future study of the mass-loss rates of O-rich AGB stars in the LMC (B. Sargent et al. 2010, in preparation) by construction of large model grids covering a range of model parameters.

4.2. Dust Temperature and Inner Radius

SSTSAGE052206 and HV 5715 have dust temperatures at the innermost radii, R_{min} , of their dust shells of 900 K and 430 K, respectively. Based on the uncertainties of R_{min} for each of the two stars, the allowable range of temperatures at dust shell inner radius for SSTSAGE052206 is 1200–700 K, and the allowable range for HV 5715 is 650–310 K. The dust temperatures at the dust shell inner radius for SSTSAGE052206 and HV 5715 are comparable to the dust temperatures at innermost dust shell radius of 1000 K (Bedijn 1987), \sim 900 K (Schutte & Tielens 1989), and 400–700 K (Simpson 1991; Suh 2004; Heras & Hony 2005) in their RT models of O-rich AGB stars. The dust shell inner radius of 17 R_{star} for SSTSAGE052206 is close to but just above the allowable range of dust shell inner radii for O-rich AGB stars (2.5–14 R_{star}) according to Höfner (2007). Observations of O-rich AGB stars' dust shell inner radii indicate smaller radii of 3–6 R_{star} (Bester et al. 1991; Danchi et al. 1995). On the other hand, modeling by Suh (2004) suggests low mass-loss rate O-rich AGBs (LMOAs) of similar luminosities to that of SSTSAGE052206 have much larger dust shell inner radii of 27–41 R_{star} . As discussed at the end of Section 3.2, if we were to include the water vapor emission in our model of SSTSAGE052206, we would need to lower the 5–8 μm flux in the model slightly. Keeping τ_{10} , a_{min} , and a_0 approximately

the same as their current values, this would mean R_{\min} would need to increase slightly.

The dust shell inner radius for HV 5715 is $52 R_{\text{star}}$, much larger than that for SSTSAGE052206. van Loon et al. (2005) found the O-rich AGB stars and red supergiants (RSGs) with higher stellar effective temperatures and greater luminosities (or greater masses, comparing their Figures 12 and 14) had larger dust-free inner cavities. The stellar effective temperatures of HV 5715 and SSTSAGE052206 assumed for our modeling of 3500 K and 3700 K, respectively, are close, while their luminosities of $\sim 36,000 L_{\odot}$ and $5100 L_{\odot}$, respectively, suggest the relatively larger dust shell inner radius HV 5715 to be consistent with the van Loon et al. (2005) result. Interferometric observations also tend to support more massive or luminous stars having relatively larger dust shell inner radii. Ohnaka et al. (2008) found the $40 M_{\odot}$ LMC RSG WOH G64 to have a dust shell inner radius of $15 R_{\text{star}}$ and a dust temperature there of 880 K. Using $11 \mu\text{m}$ interferometry, Bester et al. (1991) found the hottest dust around the Milky Way RSG α Ori to be ~ 300 K, and Danchi et al. (1995) found α Ori and the supergiants α Sco and α Her to have dust shell inner radii near $\sim 38 R_{\text{star}}$, also using $11 \mu\text{m}$ interferometry. The temperature of the dust at the inner radius of the dust shell for HV 5715 of 430 K is lower than the expected condensation temperature of ~ 900 K according to Schutte & Tielens (1989), but Wada et al. (2003) found amorphous silicates condensing at temperatures as low as ~ 650 K in laboratory experiments. We note that it may be possible to raise the dust grain temperatures at the inner radius of the shell by decreasing the thickness of the dust shell (Speck et al. 2009). However, we further note from our earlier discussions that our model of HV 5715 is likely more characteristic of it during one of its maxima. During minima in its light curve, HV 5715 is probably at least 15% fainter (see Section 3.1), so if the dust shell has not changed its dimensions, the temperature at the dust shell inner radius would be lower, due to the lower incoming flux from the star.

4.3. Dust Mass-loss Rates

Justtanont et al. (2004) found when constructing models of the SED of W Hya that the inferred mass-loss rate was not very sensitive to whether the dust properties were those of the amorphous pyroxene used in this study or the empirically constructed “astronomical silicates” used by Justtanont & Tielens (1992) or Laor & Draine (1993). This study has found the output model SED fluxes to be fairly insensitive to a_{\min} and a_0 , for the choice of Ossenkopf et al. (1992) complex indices of refraction used here. The values for these parameters used in this study, 0.01 and $0.1 \mu\text{m}$, respectively, are chosen to be similar to ranges used in other modeling studies of AGB stars. Justtanont & Tielens (1992) used grains in radius between 0.005 and $0.25 \mu\text{m}$ to model OH/IR stars (this range was also used by Justtanont et al. 2004, to model the O-rich AGB star W Hya). Kemper et al. (2001) and Kemper et al. (2002) used a range of 0.1 – $1 \mu\text{m}$ to model O-rich AGB stars.

The dust mass-loss rates obtained from the **2D**dust models for SSTSAGE052206 and HV 5715 are, respectively, $2.0 \times 10^{-9} M_{\odot} \text{yr}^{-1}$ and $2.3 \times 10^{-9} M_{\odot} \text{yr}^{-1}$. From the allowable ranges of optical depth, R_{\min} , and grain sizes, the dust mass-loss rate for SSTSAGE052206 could range from $(1.1$ – $3.3) \times 10^{-9} M_{\odot} \text{yr}^{-1}$, and the same for HV 5715 could range from $(1.1$ – $4.1) \times 10^{-9} M_{\odot} \text{yr}^{-1}$. If the shell expansion velocity for either of these two O-rich AGBs is different, the mass-loss rate would vary in a linearly dependent fashion on the expansion

velocity. Compared to dust mass-loss rates given in the literature for other O-rich AGB stars, the rates for SSTSAGE052206 and HV 5715 are reasonable. The dust mass-loss rates computed by Justtanont & Tielens (1992) for OH/IR stars with $\tau_{9.7}$ most similar to τ_{10} of ~ 0.1 and ~ 0.01 for the models of SSTSAGE052206 and HV 5715, respectively, in this study are quite similar. According to Justtanont & Tielens (1992), R Hor, R Cas, IRC+10523, and GX Mon have $\tau_{9.7}$ of 0.03, 0.08, 0.13, and 0.13, respectively, and dust mass-loss rates of 0.62 , 1.9 , 4.0 , and $7.2 \times 10^{-9} M_{\odot} \text{yr}^{-1}$, though they assumed a constant luminosity for all stars of $10,000 L_{\odot}$. Schutte & Tielens (1989) find a dust mass-loss rate for R Cas of $1.2 \times 10^{-9} M_{\odot} \text{yr}^{-1}$ with τ_{10} of 0.10 and a luminosity of $29,000 L_{\odot}$. For Z Cyg and o Ceti, Suh (2004) find dust mass-loss rates between 0.76 and $1.6 \times 10^{-9} M_{\odot} \text{yr}^{-1}$ for τ_{10} between 0.01 and 0.04 and luminosities between 4000 and $10,000 L_{\odot}$. Finally, using a computed $8 \mu\text{m}$ excess emission of ~ 7 mJy for SSTSAGE052206 and ~ 4 mJy for HV 5715, Figure 17 of Paper I suggests the dust mass-loss rates for SSTSAGE052206 and HV 5715 found in this study are a factor of ~ 3 greater than expected from van Loon et al. (1999) and a factor of ~ 10 greater than expected from the empirical relation of $8 \mu\text{m}$ excess emission and mass-loss rate given by Paper I.

4.4. Inferred Total Mass-loss Rates

To translate dust mass-loss rates to total mass-loss rates, a dust-to-gas mass ratio must be assumed, but the values of such ratios can be fairly uncertain (e.g., Decin et al. 2007). Various values quoted for O-rich mass-losing stars include 0.01 (for AGB stars; Kemper et al. 2003), 0.004 (for WX Psc, an AGB star; Decin et al. 2007), 0.003 (for Miras; Justtanont & Tielens 1992), and 0.002 (for VY CMa, a supergiant; Decin et al. 2006), among others. Here, we assume a value of 0.002 to be consistent with Paper I. van Loon (2006) shows how the dust-to-gas mass ratio is linearly proportional to metallicity, Z . If we assume the average dust-to-gas mass ratio of nearby O-rich AGB stars is 0.0063 (Knapp 1985; Heras & Hony 2005), and if we assume these nearby O-rich AGB stars have solar metallicity, then we would scale the dust-to-gas ratio by 0.4 (assumed metallicity of LMC; see Section 3.1) to get ~ 0.0025 . This is not far from our assumed dust-to-gas mass ratio. For a given mass percentage of Al_2O_3 , Heras & Hony (2005) obtain a spread in gas-to-dust ratios that usually varies by a factor of 10 (see their Figure 4), noting Marengo et al. (1997) found similarly large spreads in their gas-to-dust ratios. We adopt this factor of 10 in the uncertainty of the dust-to-gas ratio we use. Placing our value of 0.002 logarithmically in the center of this range, we estimate our dust-to-gas ratio could be between 0.00063 and 0.0063.

The gas-to-dust ratio assumed here gives total mass-loss rates of $1.2 \times 10^{-6} M_{\odot} \text{yr}^{-1}$ and $1.0 \times 10^{-6} M_{\odot} \text{yr}^{-1}$ for HV 5715 and SSTSAGE052206, respectively. However, due to the large uncertainty we assign to the dust-to-gas ratio we assume, these values could range between 0.2×10^{-6} and $6.5 \times 10^{-6} M_{\odot} \text{yr}^{-1}$ for HV 5715 and between 0.2×10^{-6} and $5.2 \times 10^{-6} M_{\odot} \text{yr}^{-1}$ for SSTSAGE052206. These total mass-loss rates are very close to each other, which is puzzling, given that the luminosities of the two stars differ by a factor of ~ 7 . However, we note the uncertainties on the total mass-loss rates could also be consistent with the total mass-loss rates being a factor of ~ 30 different between the two stars. This does not take into account possible extra factors arising from the dust expansion velocities for the two stars differing in actuality from their assumed value of 10 km s^{-1} . We do note, however, that even if the values of total

mass-loss rate we find are correct, it could just be a coincidence arising from modeling only two sources.

The total mass-loss rates we find for HV 5715 and SSTSAGE052206 are comparable to the gas mass-loss rates (much larger than dust mass-loss rates, so approximately equal to the total mass-loss rates) determined from OH and CO observations of the four OH/IR stars—R Hor, R Cas, IRC+10523, and GX Mon—in the Justtanont & Tielens (1992) sample with the lowest optical depths (see their Table 2). Schutte & Tielens (1989) find the total mass-loss rate for R Cas to be lower than but marginally consistent with the total mass-loss rates we find for HV 5715 and SSTSAGE052206. Over half of the stars whose SEDs were modeled by Heras & Hony (2005) have total mass-loss rates within the error bars of the rates for the two stars we model. The total mass-loss rates we determine for our two stars are between the rates inferred for the high and low mass-loss phases of WX Psc, as determined by Decin et al. (2007). The mass-loss relation found by van Loon et al. (2005) for O-rich AGB stars and RSGs predicts total mass-loss rates of $8.6 \times 10^{-6} M_{\odot} \text{ yr}^{-1}$ for HV 5715 and $7.8 \times 10^{-7} M_{\odot} \text{ yr}^{-1}$ for SSTSAGE052206, giving rates larger and smaller, respectively, than our **2D**dust modeling gives.

4.5. Mass-loss Rate and Evolutionary Status

4.5.1. HV 5715

From the assumed temperature and luminosity we used in modeling the two O-rich AGB stars studied here, rough conclusions may be drawn about the two stars' natures. According to the H-R diagram plotted in Figure 12 of van Loon et al. (2005), the main-sequence progenitor of HV 5715 should have had a stellar mass of $\sim 7 M_{\odot}$, and, as such, it should be experiencing HBB. From mass-loss formalism for AGB evolution developed by Volk & Kwok (1988), the primary period of HV 5715 of 415.97 days (see Section 2.1) and its assumed luminosity from modeling suggest a stellar mass of just above $7 M_{\odot}$, consistent with the estimate based on the H-R diagram of van Loon et al. (2005). Further consistent with the high mass of HV 5715 is its location in Figure 3 of Groenewegen & de Jong (1994), which suggests it to be more massive than the $5 M_{\odot}$ star for which tracks are plotted on the mass–luminosity plot. Assuming an absolute bolometric magnitude, M_{bol} , for the Sun of 4.74 (Cox 2000) and assuming the luminosities used in our modeling, HV 5715 has $M_{\text{bol}} = -6.65$, and SSTSAGE052206 has $M_{\text{bol}} = -4.53$. The closest data points to where HV 5715 would be plotted in Figure 27 of Groenewegen et al. (2009) are six stars for which HBB is inferred from Li detection, further supportive of HV 5715 experiencing HBB. Even further in support of the higher mass of HV 5715 is its location in the M_{bol} versus period plot (Figure 8) of Wood et al. (1992), which shows it to be located below the supergiants and above the AGB stars with no OH maser detections clustering around the $4 M_{\odot}$ track.

We consider HV 5715 to be an AGB star and not an RSG. Wood et al. (1983) note the classical luminosity limit for an AGB star is at $M_{\text{bol}} = -7.1$; however, as Sloan et al. (2008) summarize, Wood et al. (1992) note a few AGB stars can occasionally move over that limit. van Loon et al. (1999) propose a dividing line between AGB and RSG of $M_{\text{bol}} = -7.5$, while Groenewegen et al. (2009) use $M_{\text{bol}} = -8.0$ as a lower limit for the luminosity of stars they consider RSGs. Expressing the distinction between AGB and RSG in luminosity, van Loon et al. (2005) divide their sample of M stars by stating they consider the stars to be AGB if the luminosity is less than $10^{4.9}$ (79,433) L_{\odot} , though

they also note the classical AGB limit of $\sim 10^{4.73}$ (53,703) L_{\odot} . Buchanan et al. (2006) state the theoretical AGB luminosity limit to be 60,000 L_{\odot} but suggest AGBs can have luminosities slightly higher than this. As we have already noted, HV 5715 would fall in region G of the K_s versus $J-K_s$ CMD of Nikolaev & Weinberg (2000), given its 2MASS $J-K_s$ color of 1.3, which they note would make it a massive ($5-8 M_{\odot}$) AGB star. This is consistent with the main-sequence progenitor mass we estimate for it of $\sim 7 M_{\odot}$. van Loon et al. (1999) and others note that stars with initial masses greater than or equal to $8 M_{\odot}$ are typically considered RSGs. This is consistent with Figure 9 of Groenewegen et al. (2009), which shows the $8 M_{\odot}$ evolutionary track to form an upper limit on the luminosities of the AGB stars in their sample, though there are a few AGB stars above this track and a few RSGs below the track. HV 5715 would be marginally considered an RSG according to its $J-K_s$ color and epoch-1 and 2 [3.6]–[4.5] colors (-0.054 and -0.215 , respectively), according to the $J-K_s$ versus [3.6]–[4.5] color–color diagram in Figure 10 of Buchanan et al. (2009). However, in the color–color diagrams of Figure 9 of that paper, the [5.8]–[8.0] epoch-1 and 2 colors of 0.157 and 0.187, respectively, and [8.0]–[24] epoch-1 and 2 colors of 1.556 and 1.500 place HV 5715 outside of the region in each of the two diagrams labeled RSG, though it is on the side of the RSG region opposite the side adjacent to the region labeled “O AGB.” Caution is suggested, however, as the Buchanan et al. (2009) sample is only 250 sources. The luminosity of 36,000 L_{\odot} , bolometric magnitude of -6.65 , estimated mass of $7 M_{\odot}$, its colors, and its K_s magnitude suggest HV 5715 to be an AGB star, though these properties are also not far from being consistent with those of RSGs.

HV 5715 has a total mass-loss rate at least 10 times higher than those of O-rich AGBs and RSGs of comparable [3.6]–[8.0] color (epoch 1, 0.397; epoch 2, 0.257), though its error bars make it marginally consistent with them. This contrasts with HV 5715 having a total mass-loss rate at least 10 times *lower* than the rates for O-rich AGB stars of both similar luminosity in Figure 8 of van Loon et al. (2005) and similar M_{bol} in Figure 9 of van Loon et al. (1999), though, again, its error bars let it be marginally consistent with the rest of the O-rich AGB population. We note here that the spread in mass-loss rates at a given luminosity (e.g., as shown in Figure 8 of van Loon et al. 2005) is in part due to intrinsic differences between the stars at that luminosity and not only due to errors in determining the mass-loss rates. As Figure 13 of van Loon et al. (2005) shows, mass loss in evolved stars increases with both luminosity and stellar effective temperature. In Paper I, it is discussed how differences in mass-loss rate for stars at the same luminosity can be intrinsic. To summarize, HV 5715 has a total mass-loss rate that is high for its near-infrared color and low for its luminosity and bolometric magnitude, though the error bars on its total mass-loss rate make it marginally consistent with rates of O-rich AGBs and RSGs of similar near-infrared colors, luminosities, and bolometric magnitudes.

4.5.2. SSTSAGE052206

The H-R diagram plotted in Figure 12 of van Loon et al. (2005) shows SSTSAGE052206 to be more consistent with a $\sim 3 M_{\odot}$ star, so it is likely not experiencing HBB. At such a mass, it may eventually become C-rich, which would be consistent with our earlier discussion suggesting it to be currently early in its AGB phase. This lower mass for SSTSAGE052206 is also consistent with the Groenewegen & de Jong (1994) period–luminosity relation (their Figure 3), which shows the

M_{bol} of SSTSAGE052206 of -4.53 to be lower than all the tracks of the $5 M_{\odot}$ star and in the middle of the tracks of the $1.25 M_{\odot}$ star. Volk & Kwok (1988) do not plot lines for primary periods as low as that of SSTSAGE052206 of 81.24 days in their Figure 9, but approximate extrapolation of their curves down to the primary period of SSTSAGE052206 suggests a stellar mass below $4.5 M_{\odot}$. The primary period for this star is below the range plotted in Figure 27 of Groenewegen et al. (2009), but it looks in that plot to be consistent with O-rich AGB stars with no lithium detected, which implies SSTSAGE052206 is not experiencing HBB.

The mass-loss rate for SSTSAGE052206 and its bolometric magnitude place it in the middle of the region populated by C-rich AGB stars according to Figure 9 of van Loon et al. (1999); however, the error bars on its mass-loss rate also make it consistent with a couple of M-type AGB stars in the same figure. This is also true of Figure 8 of van Loon et al. (2005), which, in addition, shows SSTSAGE052206 to be also consistent, in terms of total mass-loss rate and luminosity, with two of the three MS- or S-type stars plotted in that figure. This similarity to S- or C-type AGB stars in these plots may also be consistent with the location for SSTSAGE052206 in the $Z = 0.008$ (approximately the LMC metallicity assumed here; see Section 3.1) plot of Figure 1 of Marigo et al. (2008). This location in the Marigo et al. (2008) H-R diagram suggests that in the future, SSTSAGE052206 may become a C-rich AGB star. In Figure 24 of Groenewegen et al. (2009), the total mass-loss rate of SSTSAGE052206 is quite consistent with the total mass-loss rates of O-rich AGB stars and RSGs of similar $[3.6]-[8.0]$ color (its epoch-1 color is 1.376 and its epoch-2 color is 1.301). Figure 21 of Groenewegen et al. (2009) shows SSTSAGE052206 to be most consistent in its I -band pulsation amplitude and total mass-loss rate with a number of RSGs and a couple of C-rich AGB stars in the Small Magellanic Cloud. To recap, SSTSAGE052206 has a total mass-loss rate consistent with other O-rich AGBs of similar near-infrared color and consistent with stars of mixed chemistry (M-, MS-, S-, and C-types) of similar luminosities, bolometric magnitudes, and I -band pulsation amplitudes.

5. CONCLUSIONS

In this study, we constructed detailed RT models using **2Dust** of the SEDs of two O-rich AGB stars in order to find useful dust properties to use in later modeling of the entire O-rich AGB population found by the SAGE surveys of the LMC. A similar study has determined useful dust properties to use in later modeling of the C-rich population in the SAGE LMC surveys (Paper III). We chose to model one star each from the bright and faint populations of O-rich AGB stars identified by Blum et al. (2006). We required each star to have an IRS spectrum from the SAGE-Spec program in order to model in detail the silicate emission features. We further required each star to have a red $[8.0]-[24]$ color relative to the rest of the O-rich AGB population, so that the dust emission was prominent at mid-infrared wavelengths; however, we did not want the $[8.0]-[24]$ colors to be too red, lest we choose an outlying, unusual star. From the bright O-rich AGB population we chose HV 5715, and from the faint O-rich AGB population we chose SSTSAGE052206.

We have fitted the photometry and spectroscopy of these two stars with **2Dust** SED models using the same dust properties. These properties include the use of complex indices of refraction

of oxygen-deficient silicates (Ossenkopf et al. 1992), a KMH-like grain size distribution (for more, see Section 3.1.5) with a power-law exponent, γ , of -3.5 , a_{min} of $0.01 \mu\text{m}$, and characteristic size for exponential tail-off to large sizes of $a_0 = 0.1 \mu\text{m}$. These dust grain properties represent a baseline set to use for constructing future grids of models of O-rich AGB stars to compare to the observed SAGE data. We note that the dust properties we used provide an excellent fit to the SED and spectrum of HV 5715, the bright O-rich AGB star, after taking into account its photometric variability. The fit to the SED and IRS spectrum of SSTSAGE052206, the faint O-rich AGB, is good overall. We do note the 10 and $20 \mu\text{m}$ features in the model peak longward and shortward, respectively, of the features in the data, suggesting the silicates of SSTSAGE052206 to be more silica-rich than both those of the oxygen-deficient Ossenkopf et al. (1992) silicates we use and those of HV 5715. This possible difference in dust composition will be sought in future studies of O-rich AGB stars in the LMC.

Simple models of water vapor and carbon dioxide gas emission for SSTSAGE052206 suggest negligible contribution to the near-infrared continuum flux from the carbon dioxide and at most 10% of the flux between 5 and $8 \mu\text{m}$ to come from water vapor. This suggests our modeling of the near-infrared continuum flux arising completely from dust emission is not a bad approximation. Were we to include gas emission in our dust models, we would need either to increase R_{min} slightly or to decrease any of τ_{10} , a_{min} , or a_0 slightly. We also find the large region from which the water vapor arises to be consistent with the large dust shell inner radius we find for SSTSAGE052206.

We derive $\dot{M} = 2.3 \times 10^{-6} M_{\odot} \text{yr}^{-1}$ for HV 5715 and $\dot{M} = 2.0 \times 10^{-6} M_{\odot} \text{yr}^{-1}$ for SSTSAGE052206, although the error bars on each of these of $(0.2-6.5) \times 10^{-6} M_{\odot} \text{yr}^{-1}$ and $(0.2-5.2) \times 10^{-6} M_{\odot} \text{yr}^{-1}$, respectively, are very large. We note these uncertainties arise from the uncertainties in dust mass-loss rates and the dust-to-gas mass ratios assumed. The former originate from uncertainties estimated by eye for the free parameters R_{min} , τ_{10} , a_{min} , and a_0 , which were likely conservatively estimated—the formal uncertainties on these parameters may be smaller. The latter uncertainty, that in the dust-to-gas mass ratio, contributing to the uncertainty in total mass-loss rate would be much smaller if we had detailed measurements of the gas component of these stars' circumstellar shells. We have not factored in the uncertainty in the dust expansion velocity. We believe the value we have assumed for dust expansion velocity is close to the real value for HV 5715. We have no information on the dust expansion velocity for SSTSAGE052206.

The total mass-loss rates we find for HV 5715 and SSTSAGE052206 may have very large uncertainties, but we note that the purpose of this study was not to obtain precise total mass-loss rates; instead, we seek good dust properties to use in later modeling of the entire O-rich AGB population of the SAGE surveys. By fitting the SED and spectrum of a star from each of the bright and faint populations of O-rich AGB stars (Blum et al. 2006), we intend to account for possible differences between the average dust properties of the two populations. We find good fits of our models to the data for these two stars. We also note that a major goal of SAGE is to find the relative rates of dust injection from the different sources of dust in the LMC, which includes RSGs, C-rich AGB stars and “extreme” AGB stars in addition to the bright and faint populations of O-rich AGB stars. Such does not require knowledge of total mass-loss rates, only dust mass-loss rates, which means modeling of the dust

emission from such evolved stars will be sufficient to achieve that goal. We find that the total and dust mass-loss rates, dust shell inner radii and temperatures at those radii, and other modeling parameters are consistent with those assumed and inferred by other studies of O-rich AGB stars with similar properties to each of HV 5715 and SSTSAGE052206. This gives confidence that the dust properties we find for these two stars will be useful in modeling the rest of the O-rich AGB stars in the SAGE sample.

This work is based on observations made with the *Spitzer Space Telescope*, which is operated by the Jet Propulsion Laboratory, California Institute of Technology under NASA contract 1407. We acknowledge funding from the NAG5-12595 grant, SAGE-LMC *Spitzer* grant 1275598, SAGE-SEEDS *Spitzer* grant 1310534, and Herschel/HERITAGE grant 1381522. This publication makes use of the Jena-St. Petersburg Database of Optical Constants (Henning et al. 1999). The authors wish to thank the anonymous referee for comments that greatly improved this manuscript. The authors also thank Kevin Volk, Sacha Hony, Albert Zijlstra, Jacco van Loon, and Martha Boyer for helpful comments and discussion. We wish to thank Peter Hauschildt for his assistance with the PHOENIX stellar photosphere models. The authors have made use of the SIMBAD astronomical database and thank those responsible for its upkeep. The authors also thank Bernie Shiao at STScI for his hard work on the SAGE database and his kind assistance.

REFERENCES

- Allard, F., Hauschildt, P. H., & Schweitzer, A. 2000, *ApJ*, 539, 366
- Bedijn, P. J. 1987, *A&A*, 186, 136
- Bessell, M. S., Castelli, F., & Plez, B. 1998, *A&A*, 333, 231
- Bester, M., Danchi, W. C., Degiacomi, C. G., Townes, C. H., & Geballe, T. R. 1991, *ApJ*, 367, L27
- Blommaert, J. A. D. L., et al. 2006, *A&A*, 460, 555
- Blum, R. D., et al. 2006, *AJ*, 132, 2034
- Bohren, C. F., & Huffman, D. R. 1983, *Absorption and Scattering of Light by Small Particles* (New York: Wiley)
- Boothroyd, A. I., & Sackmann, I.-J. 1992, *ApJ*, 393, L21
- Bouwman, J. 2001, PhD thesis, Astronomical Institute Anton Pannekoek, Univ. Amsterdam
- Bouwman, J., de Koter, A., van den Ancker, M. E., & Waters, L. B. F. M. 2000, *A&A*, 360, 213
- Buchanan, C. L., Kastner, J. H., Forrest, W. J., Hrivnak, B. J., Sahai, R., Egan, M., Frank, A., & Barnbaum, C. 2006, *AJ*, 132, 1890
- Buchanan, C. L., Kastner, J. H., Hrivnak, B. J., & Sahai, R. 2009, *AJ*, 138, 1597
- Cami, J. 2002, PhD thesis, Univ. Amsterdam
- Cami, J., van Malderen, R., & Markwick, A. J. 2010, *ApJS*, 187, 409
- Celis, S. L. 1978, *A&A*, 63, 53
- Cioni, M.-R. L., Girardi, L., Marigo, P., & Habing, H. J. 2006, *A&A*, 448, 77
- Cioni, M.-R. L., van der Marel, R. P., Loup, C., & Habing, H. J. 2000, *A&A*, 359, 601
- Cohen, M., Wheaton, W. A., & Megeath, S. T. 2003, *AJ*, 126, 1090
- Cornette, W. M., & Shanks, J. G. 1992, *Appl. Opt.*, 31, 3152
- Cousins, A. W. J. 1976, *MmRAS*, 81, 25
- Cox, A. N. 2000, *Allen's Astrophysical Quantities* (4th ed.; New York: Springer-Verlag)
- Danchi, W. C., Bester, M., Greenhill, L. J., Degiacomi, C. G., Geis, N., Hale, D., Lopez, B., & Townes, C. H. 1995, *Ap&SS*, 224, 447
- Decin, L., Hony, S., de Koter, A., Justtanont, K., Tielens, A. G. G. M., & Waters, L. B. F. M. 2006, *A&A*, 456, 549
- Decin, L., Hony, S., de Koter, A., Molenberghs, G., Dehaes, S., & Markwick-Kemper, F. 2007, *A&A*, 475, 233
- Dorschner, J., Begemann, B., Henning, T., Jaeger, C., & Mutschke, H. 1995, *A&A*, 300, 503
- Draine, B. T., & Lee, H. M. 1984, *ApJ*, 285, 89
- Egan, M. P., Leung, C. M., & Spagna, G. F., Jr. 1988, *Comput. Phys. Commun.*, 48, 271
- Fabian, D., Henning, T., Jäger, C., Mutschke, H., Dorschner, J., & Wehrhan, O. 2001, *A&A*, 378, 228
- Fazio, G. G., et al. 2004, *ApJS*, 154, 10
- Feast, M. 1999, *PASP*, 111, 775
- Fraser, O. J., Hawley, S. L., & Cook, K. H. 2008, *AJ*, 136, 1242
- Fraser, O. J., Hawley, S. L., Cook, K. H., & Keller, S. C. 2005, *AJ*, 129, 768
- Gail, H.-P., Zhukovska, S. V., Hoppe, P., & Trieloff, M. 2009, *ApJ*, 698, 1136
- Glass, I. S. 1979, *MNRAS*, 186, 317
- Groenewegen, M. A. T., & de Jong, T. 1994, *A&A*, 288, 782
- Groenewegen, M. A. T., Sloan, G. C., Soszyński, I., & Petersen, E. A. 2009, *A&A*, 506, 1277
- Harrington, J. P., Monk, D. J., & Clegg, R. E. S. 1988, *MNRAS*, 231, 577
- Henning, T., Il'In, V. B., Krivova, N. A., Michel, B., & Voshchinnikov, N. V. 1999, *A&AS*, 136, 405
- Heras, A. M., & Hony, S. 2005, *A&A*, 439, 171
- Höfner, S. 2007, in ASP Conf. Ser. 378, *Why Galaxies Care About AGB Stars: Their Importance as Actors and Probes*, ed. F. Kerschbaum, C. Charbonnel, & R. Wing (San Francisco, CA: ASP), 145
- Höfner, S. 2009, in AIP Conf. Ser. 1094, *Cool Stars 15: The 15th Cambridge Workshop on Cool Stars, Stellar Systems, and the Sun*, ed. E. Stempels (Melville, NY: AIP), 872
- Houck, J. R., et al. 2004, *ApJS*, 154, 18
- Ivezic, Z., Nenkova, M., & Elitzur, M. 1999, User Manual for DUSTY, Univ. of Kentucky Internal Report (<http://www.pa.uky.edu/~moshe/dusty>)
- Jaeger, C., Mutschke, H., Begemann, B., Dorschner, J., & Henning, T. 1994, *A&A*, 292, 641
- Jäger, C., Dorschner, J., Mutschke, H., Posch, T., & Henning, T. 2003, *A&A*, 408, 193
- Justtanont, K., de Jong, T., Tielens, A. G. G. M., Feuchtgruber, H., & Waters, L. B. F. M. 2004, *A&A*, 417, 625
- Justtanont, K., Feuchtgruber, H., de Jong, T., Cami, J., Waters, L. B. F. M., Yamamura, I., & Onaka, T. 1998, *A&A*, 330, L17
- Justtanont, K., & Tielens, A. G. G. M. 1992, *ApJ*, 389, 400
- Justtanont, K., et al. 2005, *A&A*, 439, 627
- Kato, D., et al. 2007, *PASJ*, 59, 615
- Kemper, F., de Koter, A., Waters, L. B. F. M., Bouwman, J., & Tielens, A. G. G. M. 2002, *A&A*, 384, 585
- Kemper, F., Stark, R., Justtanont, K., de Koter, A., Tielens, A. G. G. M., Waters, L. B. F. M., Cami, J., & Dijkstra, C. 2003, *A&A*, 407, 609
- Kemper, F., Waters, L. B. F. M., de Koter, A., & Tielens, A. G. G. M. 2001, *A&A*, 369, 132
- Kemper, F., et al. 2010, *PASP*, in press (arXiv:1004.1142)
- Kim, S.-H., Martin, P. G., & Hendry, P. D. 1994, *ApJ*, 422, 164
- Knapp, G. R. 1985, *ApJ*, 293, 273
- Laor, A., & Draine, B. T. 1993, *ApJ*, 402, 441
- Leung, C. M. 1975, *ApJ*, 199, 340
- Leung, C. M. 1976a, *J. Quant. Spectrosc. Radiat. Transfer*, 16, 559
- Leung, C. M. 1976b, *ApJ*, 209, 75
- Marengo, M., Canil, G., Silvestro, G., Origlia, L., Busso, M., & Persi, P. 1997, *A&A*, 322, 924
- Marigo, P., Girardi, L., Bressan, A., Groenewegen, M. A. T., Silva, L., & Granato, G. L. 2008, *A&A*, 482, 883
- Markwick, A. J., & Millar, T. J. 2000, *A&A*, 359, 1162
- Marshall, J. R., van Loon, J. T., Matsuura, M., Wood, P. R., Zijlstra, A. A., & Whitelock, P. A. 2004, *MNRAS*, 355, 1348
- Mathis, J. S., Ruml, W., & Nordsieck, K. H. 1977, *ApJ*, 217, 425
- Matsuura, M., Yamamura, I., Cami, J., Onaka, T., & Murakami, H. 2002, *A&A*, 383, 972
- Meixner, M., et al. 2006, *AJ*, 132, 2268
- Min, M., Hovenier, J. W., & de Koter, A. 2005, *A&A*, 432, 909
- Nikolaev, S., & Weinberg, M. D. 2000, *ApJ*, 542, 804
- Nittler, L. R. 2009, *PASA*, 26, 271
- Ohnaka, K., Driebe, T., Hofmann, K.-H., Weigelt, G., & Wittkowski, M. 2008, *A&A*, 484, 371
- Ossenkopf, V., Henning, T., & Mathis, J. S. 1992, *A&A*, 261, 567
- Partridge, H., & Schwenke, D. W. 1997, *J. Chem. Phys.*, 106, 4618
- Pettit, E., & Nicholson, S. B. 1933, *ApJ*, 78, 320
- Rebeiro, E., Martin, N., Prevot, L., Robin, A., Peyrin, Y., Mianes, P., & Rousseau, J. 1983, *A&AS*, 51, 277
- Reid, M. J., & Goldston, J. E. 2002, *ApJ*, 568, 931
- Rieke, G. H., et al. 2004, *ApJS*, 154, 25
- Rothman, L. S., et al. 2005, *J. Quant. Spectrosc. Radiat. Transfer*, 96, 139
- Schlegel, D. J., Finkbeiner, D. P., & Davis, M. 1998, *ApJ*, 500, 525
- Schultheis, M., Lançon, A., Omont, A., Schuller, F., & Ojha, D. K. 2003, *A&A*, 405, 531
- Schutte, W. A., & Tielens, A. G. G. M. 1989, *ApJ*, 343, 369
- Simpson, J. P. 1991, *ApJ*, 368, 570
- Skrutskie, M. F., et al. 2006, *AJ*, 131, 1163
- Sloan, G. C., Kraemer, K. E., Goebel, J. H., & Price, S. D. 2003, *ApJ*, 594, 483

- Sloan, G. C., Kraemer, K. E., Wood, P. R., Zijlstra, A. A., Bernard-Salas, J., Devost, D., & Houck, J. R. 2008, *ApJ*, **686**, 1056
- Smak, J. 1964, *ApJS*, **9**, 141
- Soszyński, I., et al. 2009, *Acta Astron.*, **59**, 239
- Spagna, G. F., Jr., & Leung, C. M. 1983, *Comput. Phys. Commun.*, **28**, 337
- Speck, A. K., Corman, A. B., Wakeman, K., Wheeler, C. H., & Thompson, G. 2009, *ApJ*, **691**, 1202
- Srinivasan, S. 2009, PhD Thesis, Johns Hopkins University (arXiv:0911.0799)
- Srinivasan, S., et al. 2009, *AJ*, **137**, 4810 (Paper I)
- Srinivasan, S., et al. 2010, *A&A*, submitted
- Suh, K.-W. 1999, *MNRAS*, **304**, 389
- Suh, K.-W. 2004, *ApJ*, **615**, 485
- Tokunaga, A. T., & Vacca, W. D. 2005, *PASP*, **117**, 421
- Tsuji, T. 2001, *A&A*, **376**, L1
- Tsuji, T., Ohnaka, K., Aoki, W., & Yamamura, I. 1997, *A&A*, **320**, L1
- Ueta, T., & Meixner, M. 2003, *ApJ*, **586**, 1338
- van Loon, J. T. 2006, in ASP Conf. Ser. 353, *Stellar Evolution at Low Metallicity: Mass Loss, Explosions, Cosmology*, ed. H. Lamers, et al. (San Francisco, CA: ASP), 211
- van Loon, J. Th., Cioni, M.-R. L., Zijlstra, A. A., & Loup, C. 2005, *A&A*, **438**, 273
- van Loon, J. Th., Groenewegen, M. A. T., de Koter, A., Trams, N. R., Waters, L. B. F. M., Zijlstra, A. A., Whitelock, P. A., & Loup, C. 1999, *A&A*, **351**, 559
- Vassiliadis, E., & Wood, P. R. 1993, *ApJ*, **413**, 641
- Vijh, U. P., et al. 2009, *AJ*, **137**, 3139
- Volk, K., & Kwok, S. 1988, *ApJ*, **331**, 435
- Wada, S., Murata, Y., Tokunaga, A. T., & Watanabe, J. 2003, *A&A*, **406**, 783
- Werner, M. W., et al. 2004, *ApJS*, **154**, 1
- Westerlund, B. E. 1997, *The Magellanic Clouds* (Cambridge: Cambridge Univ. Press)
- Wood, P. R., Bessell, M. S., & Fox, M. W. 1983, *ApJ*, **272**, 99
- Wood, P. R., Whiteoak, J. B., Hughes, S. M. G., Bessell, M. S., Gardner, F. F., & Hyland, A. R. 1992, *ApJ*, **397**, 552
- Wood, P. R., et al. 1999, in IAU Symp. 191, *Asymptotic Giant Branch Stars*, ed. E. Le Bertre, A. Lébre, & C. Waelkens (San Francisco, CA: ASP), 151
- Zaritsky, D., Harris, J., & Thompson, I. 1997, *AJ*, **114**, 1002